

Performance of the GSN station KIP-IU, 1988-2009

A report in a series documenting the status of the Global Seismographic Network

WQC Report 2010:2
January 7, 2010

Göran Ekström and Meredith Nettles

Waveform Quality Center
Lamont-Doherty Earth Observatory of Columbia University, New York

1 Station performance report: KIP

This report summarizes a number of observations that are relevant for assessing the past and current quality of the data recorded at one of the stations of the Global Seismographic Network. The purpose of the report is, in part, to document specific problems observed with the data. Some of these problems are related to errors in the available descriptions of station parameters: orientation of the sensors, response functions, polarities. In principle, such errors in the station metadata can be corrected by providing updated station parameters. In practice, this may be difficult in some cases due to lack of knowledge of, or inability to determine, the correct parameters. Other problems are caused by the malfunctioning of some instrument component. Regardless of the cause, it is necessary to document and publicize the lack of accurate and reliable station characteristics, especially when it is not obvious from simple inspection of the data that a problem exists.

1.1 Station KIP

The station KIP (Kipapa) is located in the interior of Oahu, Hawaii, in the central Pacific (see Figure 1). It is in an excellent location for providing global coverage in earthquake and Earth structure studies. The closest GSN station is POHA-IU (Pohakuloa), located on the island of Hawaii, approximately 300 km southeast of KIP.

KIP is part of the USGS (IU) component of the IRIS/USGS Global Seismographic Network. KIP is also a station of the Geoscope (G) network.

1.2 The data

Digital seismic data from KIP are available from the IRIS DMC beginning in 1988. The initial installation consisted of a set of STS-1 seismometers. An auxiliary STS-2 sensor was installed in 1999. Data from KIP are included in our standard CMT analysis (Dziewonski et al., 1981; Ekström et al., 2005), and waveform data, travel-time observations, and dispersion curves derived from KIP data have been used in the development of numerous global and regional tomographic models since the station was installed.

In the analyses described here, we have made use of data collected from the IRIS DMC. We requested and downloaded all long-period (LH) and very-long-period (VH) data available at the DMC for both sensors

from the start of operation (1988) until the second half of 2009. We used the currently available station metadata prepared by the Albuquerque Seismological Laboratory and available at the IRIS DMC (downloaded in December 2009). Overall, the station has been operated with few data outages since 1988.

1.3 The metadata

The dataless SEED volume for KIP documents 7 response epochs for the STS-1 (primary) and STS-2 (secondary) sensors at KIP. The STS-1 1 sps channels were initially called LHZ, LHN, LHE, without a location code. They were renamed with the location code 00 on 1999.045 (045 representing the julian day). We refer to these channels as LHZ-00, LHN-00, and LHE-00. The STS-2 sensor (location code 10) was installed on 1999.045 and we refer to the 1 sps channels as LHZ-10, LHN-10, and LHE-10. Epoch boundaries are given at 1988.228 (first data), 1990.276 (end of reversed-polarity epoch), 1994.090, 1995.210, 1999.045, 2006.144, and 2009.211. The metadata indicate no changes in gain or frequency characteristics during the period 1988–2009.

1.4 Scaling analysis

One method for assessing the quality of the data is the systematic comparison of recorded long-period waveforms with synthetic seismograms calculated for known seismic events. This analysis follows the steps described by Ekström et al. (2006). Seismic data for the LH and VH channels from both the STS-1 and STS-2 sensors are collected. Corresponding synthetic waveforms for all earthquakes in the Global CMT catalog (Dziewonski et al., 1981; Ekström et al., 2005) with $M_W \geq 6.5$ are calculated. Correlation coefficients and optimal scaling factors between observed and synthetic waveforms are calculated for the three types of data used in the standard CMT analysis: body waves (B), with periods in the range 50–150 sec, mantle waves (M), with periods in the range 125–350 sec, and surface waves (S), with periods in the range 50–150 sec. The scaling factor is only calculated for waveforms with a correlation of 0.75 or greater. The scaling factor is the number by which the synthetic seismogram should be multiplied to maximize the agreement with the observed seismogram. Annual averages of the scaling factors are calculated when four or more individual event scaling estimates are available for the year. Reversed components can be identified by their large negative correlations.

Figure 2 shows the results of our systematic comparison of KIP waveforms with synthetic seismograms. The diagrams show some periods with erratic scaling between data and synthetics, as well as a general trend towards scaling factors smaller than unity. A subset of the components appear to have had reversed polarity (with respect to that given in the metadata) during part the time period 1988–1990. All channels are affected, but not necessarily at the same time.

The clearest indications of sensor problems exist for the vertical and horizontal components of the STS-1 since 2003. The mantle-wave scaling factor for the vertical component dropped dramatically during the period 2003–2006, as previously reported by Ekström et al. (2006), and a similar trend is seen in the East-West and, less clearly, the North-South data. The pattern is repeated in the East-West data in 2008–present. The STS-2 scaling appears internally consistent throughout the period of operation (1999–present).

1.5 Noise analysis

A second method for investigating the overall performance of the sensors is to monitor background noise levels for all seismic channels, after conversion of the data to ground acceleration. We calculate hourly rms values of the time-domain seismic signal in narrow frequency bands, and convert the rms values to a power spectral density (PSD) at that frequency using Parseval’s theorem. For each month, we then calculate the low-noise value at each frequency by determining the PSD amplitude not exceeded 10% of the time.

The PSD data provide a wealth of information about the station and the sensors. Figure 3 shows the monthly low-noise estimate for each LH channel at 72 s period since 1988. The first observation is that the station has been providing data without major outages since 1988. Only in 1989 and 1993–1994 are there gaps of a few months. Second, the noise data suggest that KIP generally is a very quiet site, and that the noise characteristics have remained stable during the 22 years of operation, especially on the vertical component. Third, the STS-2 noise levels are similar to those of the STS-1 (at this period).

However, noise levels for the STS-1 horizontal components have been high since 2008. The very low noise levels shown by the STS-1 vertical component (LHZ-00) in 2005 coincide with the period of anomalous scaling seen in Figure 2.

1.6 Inter-sensor coherence

An additional method for assessing the quality and calibration of the recorded signals is to calculate inter-sensor coherence. This analysis is possible when more than one sensor is operated in the same location. At KIP, this is possible for the period 1999–2009, during which time both STS-1 and STS-2 instruments have been operating.

We calculate the coherence of the deconvolved vertical, N–S, and E–W components. The coherence is calculated for ~ 2 -hour-long time windows containing the signals for earthquakes with $M_W \geq 6.5$ (the same events used in the scaling analysis). For each pair of seismograms, the coherence is calculated in narrow frequency bands around 32 s, 64 s, 128 s and 256 s. If the coherence is greater than 0.95, the value is stored together with the complex scaling factor (represented here as a scaling factor and phase shift) that should be applied to the secondary-sensor data to bring the two time series into the best agreement. In the following, the discussion is based on the assumption that the secondary (STS-2) sensor is properly calibrated and that deviations from a scaling factor of 1.0 and a phase shift of 0° should be attributed to differences between the true and reported response functions of the primary (STS-1) sensor.

Figure 4 shows the results of the coherence analysis for the vertical component. For the period 1999–2006, significant problems are obvious. For the period 1999–2003, the gain at 256 s is too small by 10–15%. Then, starting in 2003, there is a gradual loss of long-period gain that persists until 2006. The loss of gain is accompanied by a phase shift, largest at 128 s period. In 2006, the instrument characteristics change, and for the recent period (2006–2009) the only detectable difference between the STS-1 and STS-2 vertical components from this analysis is an $\sim 5\%$ offset in the gain at all frequencies.

The horizontal components show results that are similar to those of the vertical, but less dramatic. Figure 5 shows the amplitude and phase differences for the N–S components. A gradual loss of long-period gain is seen during the period 2004–2006. Since 2006, the frequency response appears correct, and the only detectable problem is a 5–10% offset in the gain at all frequencies. It is not clear to us why the scatter in the scaling and phase-shift values at a given frequency appears to be smaller in recent years.

Figure 6 shows the results for the E–W component. During the period 1999–2002, the gain is 10% too small at 32 s period. The frequency response appears correct during 2002–2004. We observe a gradual loss of long-period gain during 2004–2006. After a step-like improvement in 2006, the loss of long-period gain recommenced and is severe for the latest data shown in the graph. In addition, a frequency-independent offset in gain with respect to the STS-2 of $\sim 10\%$ appears to have been introduced in 2006.

We also note that some of the times of sudden changes in the responses, seen in the coherence plots but not reflected in the metadata, are associated with station visits. For example, KIP was visited several times in late 2005 and early 2006 (personal communication from Bob Hutt).

1.7 Polarization analysis

The orientation of the horizontal components can be assessed empirically by comparing observed and synthetic waveforms, and finding the angle by which the horizontal components should be rotated in order to maximize the agreement. We follow the approach described by Ekström and Busby (2008) for such a comparison, using the observed and synthetic waveforms from Global CMT analysis.

We apply the method of Ekström and Busby (2008) to the same dataset used in the scaling analysis. Figure 7 shows the individual measurements for the period of operation for the different channels. Overall, the number of useful observations is large, a consequence of the low level of horizontal noise at KIP. No polarization observations are obtained for 1988–1989 since at least one horizontal component was reversed in polarity during this time period. The median rotation angles for the STS-1 and the STS-2 sensors are both 1° , and the spreads of observations are small. The median estimates for the entire period of operation are given in Table 1.

| Comp. 1 | Comp. 2 | First | Last | # Obs. | N | Az 1 | Az 2 | 25% | Med. | 75% |
|---------|---------|----------|----------|--------|-----|------|------|-----|------|-----|
| LHE | LHN | 19880820 | 19990128 | 294 | 88 | 90 | 0 | -2 | 1 | 4 |
| LHE-00 | LHN-00 | 19990304 | 20090623 | 421 | 158 | 90 | 0 | -1 | 1 | 4 |
| LHE-10 | LHN-10 | 19990304 | 20090623 | 419 | 159 | 90 | 0 | -2 | 1 | 3 |

Table 1: Statistics of sensor-rotation angles estimated in this study. Columns are the channel names, the dates of the first and last observations considered in making the estimate, the total number of observations, the number of observations of acceptable quality, the reported azimuths of sensitivity of the two channels, the median polarization-angle deviation from the reported orientation together with the range of the second (25%) and third (75%) quartiles of the observations.

1.8 Example seismograms

The anomalies described here agree with observations we have made in our routine analysis of waveforms for the determination of CMT earthquake parameters. When confronted with the seismograms for an individual earthquake, it is often difficult to assess whether a poor fit is due to incorrect source parameters, inadequate modeling of wave propagation through an Earth model, or some problem with the recorded seismograms. Here, we have included some examples of data that illustrate the characteristics of the types of problems that we have encountered with data from the KIP station.

Figure 8 shows an example of three-component mantle-wave data for an earthquake on September 4, 1989. All components are reversed in polarity, reflecting an apparent problem with the metadata during the first two years of operation. The metadata indicate that all instrument components were reversed with respect to standard orientations during the epoch 1988.228–1990.276, but the data suggest that the instrument had normal polarities at the time of this earthquake. Apart from the reversed polarities, the data are well matched.

The top panel of Figure 9 shows a comparison between mantle-wave seismograms recorded on the STS-1 seismometer and the corresponding synthetic waveforms for an event on April 7, 2009. Both the amplitude and the phase of the waveforms are poorly matched on the East-West component, indicating an error in the STS-1 response function. The bottom panel of Figure 9 shows the comparison between seismograms recorded on the STS-2 seismometer and the corresponding synthetic waveforms for the same event. For this sensor the fit is good for all components.

2 Summary and analysis

At the time of writing (January, 2010), the GSN station KIP is not performing well. The response of the East-West component of the STS-1 sensor appears to be gradually deteriorating in a similar manner to that observed on all three components in 2006. While the vertical and North-South components appear to have stable relative responses, based on the coherence analysis, both show differences of 5–10% in the absolute response with respect to the STS-2 sensor at the current time.

The coherence analysis suggests that the relative response of the vertical component has been correct only for the time period 2006–2009, and that very large time-dependent changes in the response affected the period 2003–2006. The scaling analysis (Figure 2) suggests that time-dependent response changes may also have occurred during the period before a secondary sensor was installed. For example, the response during 1991–1993 may be different from 1994–1995, based on the scaling analysis.

The horizontal components of the STS-1 sensor appear to have malfunctioned in a manner similar to that of the vertical component. That is, a gradual loss of long-period gain has occurred over a period of one to several years, with the pattern repeating more than once.

Vertical and horizontal noise levels on both the STS-1 and STS-2 sensors are generally low and quite similar in magnitude, suggesting that the use of data from the STS-2 may be possible until the problems with the primary sensor are addressed.

Our scaling analysis (Figure 2) suggests that the polarity of the recorded signals changed several times during the period 1988–1990. This appears to be the only serious problem with the data during this time period.

3 Conclusions and recommendations

This analysis shows that KIP is not currently generating data of GSN quality. In particular, neither the relative nor absolute calibrations appear to be known to better than $\sim 10\%$ for the vertical and North-South components. The East-West component of the STS-1 sensor is also malfunctioning. Unfortunately, the time-dependence of the frequency-response functions for all STS-1 components over the last decade, revealed by the coherence analysis, makes it unlikely that any retroactive remedy for the observed problems will be possible. The earlier data (pre-1999) may have been affected in a similar way.

The sensor problems identified here should have been identified early on, and corrected. We speculate that the problem went unnoticed or undiagnosed because no routine calibrations are performed at GSN stations. The lack of systematic calibrations, and inspection of calibration results, makes it difficult to identify instrument problems. In addition, the lack of calibrations makes it nearly impossible to repair errors in instrument parameters once a problem has been identified. The symptoms of the STS-1 malfunction are similar to those observed at other stations (Ekström et al., 2006); interpretation is complicated by the presence of multiple sensor problems.

Modern seismological analyses require well-calibrated instruments. Amplitude variations of 10% and smaller are interpreted as signals in modern studies that seek to map the attenuating properties of the Earth's interior (e.g., Dalton and Ekström, 2006). Phase anomalies of a few seconds at long periods are similarly interpreted in terms of Earth's elastic structure by numerous authors. Data from KIP have been used in such studies with the assumption that the station is meeting GSN design goals (IRIS, 1985; Lay et al., 2002) with respect to instrument stability. Clearly it does not, and its failure to do so should be documented. This is particularly important when, as for KIP, the data may appear visually to be correct, but are actually faulty.

It is urgent to restore KIP to a state where it generates GSN-quality data. It is fortunate that the STS-2 appears to have been providing high-quality replacement data during the last 10 years. It would be useful to publicize the fact that for much of this time period (and at present), the data from the secondary sensor may be of higher quality than those from the primary sensor.

4 References

- Dalton, C. A., and G. Ekström, Global models of surface wave attenuation, *J. Geophys. Res.*, 111, B05317, 2006.
- Dziewonski, A. M., T.-A. Chou, and J. H. Woodhouse, Determination of earthquake source parameters from waveform data for studies of global and regional seismicity, *J. Geophys. Res.*, 86, 2825–2853, 1981.
- Ekström, G., A. M. Dziewonski, N. N. Maternovskaya, and M. Nettles, Global seismicity of 2003: Centroid-moment tensor solutions for 1087 earthquakes, *Phys. Earth Planet. Inter.*, 148, 327–351, 2005.
- Ekström, G., C. A. Dalton, and M. Nettles, Observations of time-dependent errors in long-period gain at global seismic stations, *Seism. Res. Lett.*, 77, 12–22, 2006.
- Ekström, G., and R. W. Busby, Measurements of seismometer orientation at USArray Transportable and Backbone stations, *Seism. Res. Lett.*, 79, 554-561, 2008.
- IRIS, *The design goals for a new global seismographic network*, IRIS GSN committee report, 31 pages, 1985.
- Lay, T., J. Berger, R. Buland, R. Butler, G. Ekström, B. Hutt, B. Romanowicz, *Global seismic network design goals update 2002*, IRIS GSN committee report, 2002.
- Nettles, M., and G. Ekström, Glacial earthquakes in Greenland and Antarctica, *Annual Reviews*, in review, 2010.
- Peterson, J., Observations and modeling of background seismic noise, *U. S. Geol. Surv. Open-file Rep.* 93-322, 1–45, 1993.

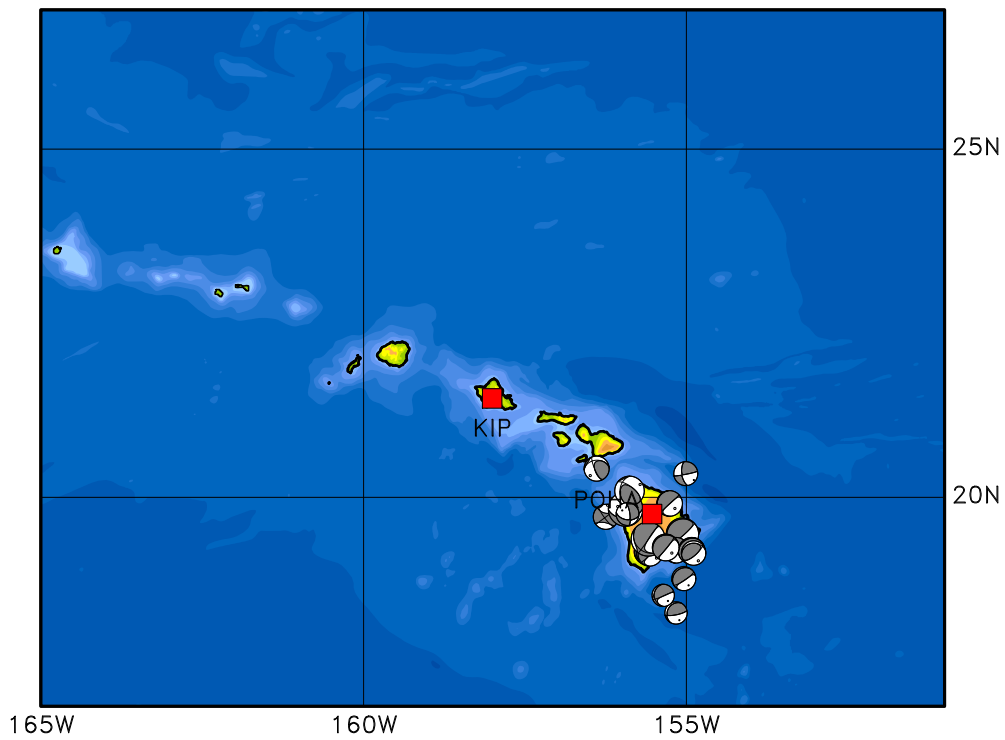


Figure 1: Map showing the location of KIP (northern red square) on the island of Oahu. Grey focal mechanisms show the locations and moment tensors of earthquakes in the Global CMT catalog. The closest GSN station is POHA, located to the southeast on the island of Hawaii.

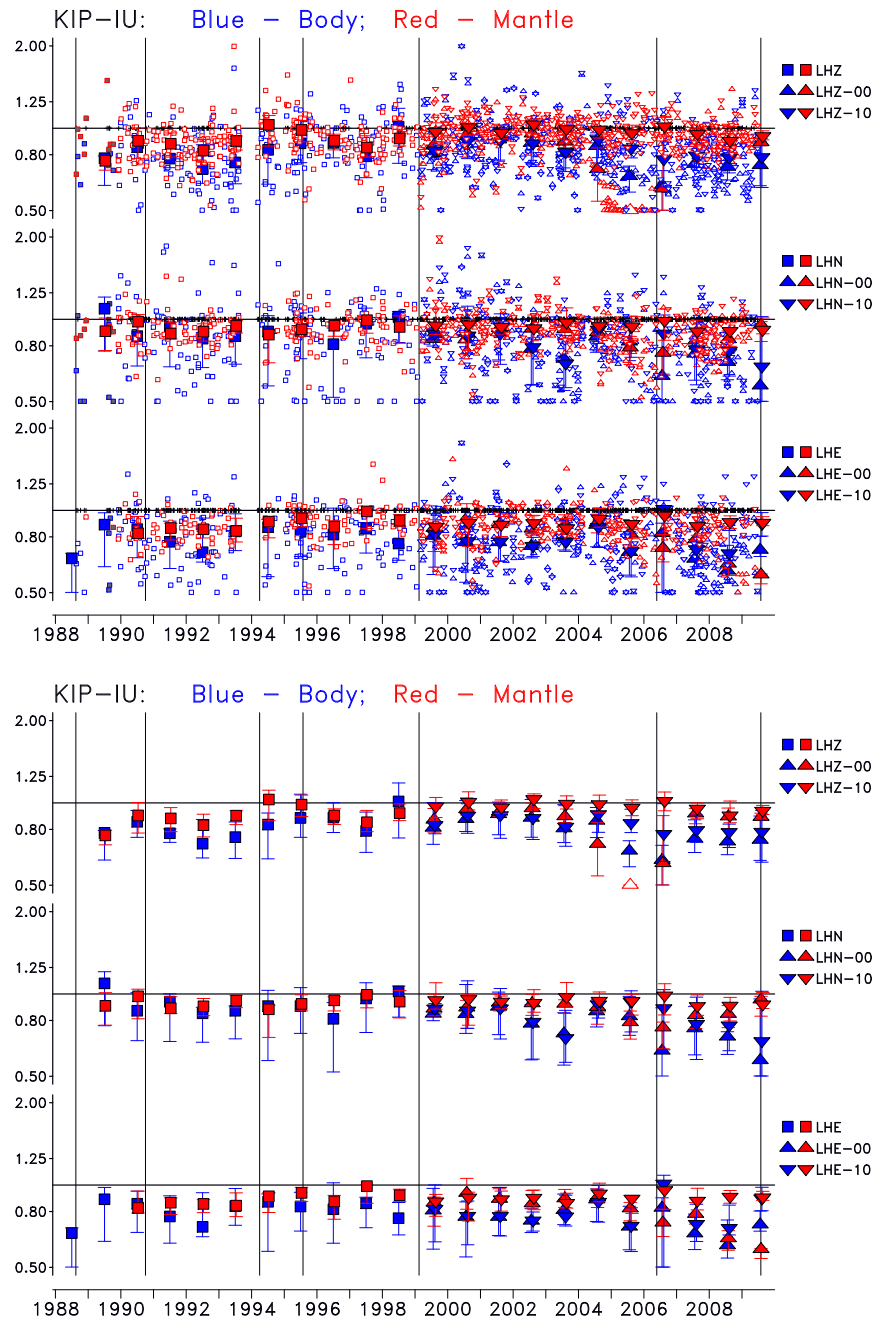


Figure 2: Scaling factors for the different data channels at KIP. Small symbols in top panel show scaling factors for individual traces. Tick marks on the horizontal axes show times of observations for which the correlation was less than 0.75. Large symbols show the median scaling factor for each year, with the error bars corresponding to the range of the second and third quartiles of the scaling factors. The legend on the right identifies the symbol type with a specific channel. Open large symbols indicate that the annual scaling factor was smaller than 0.5. Small filled symbols indicate individual traces with good correlation but reversed polarity (e.g., in 1988–1990). Thin vertical lines show the response epoch boundaries present in the metadata. Bottom panel: same, but showing only the annual median values.

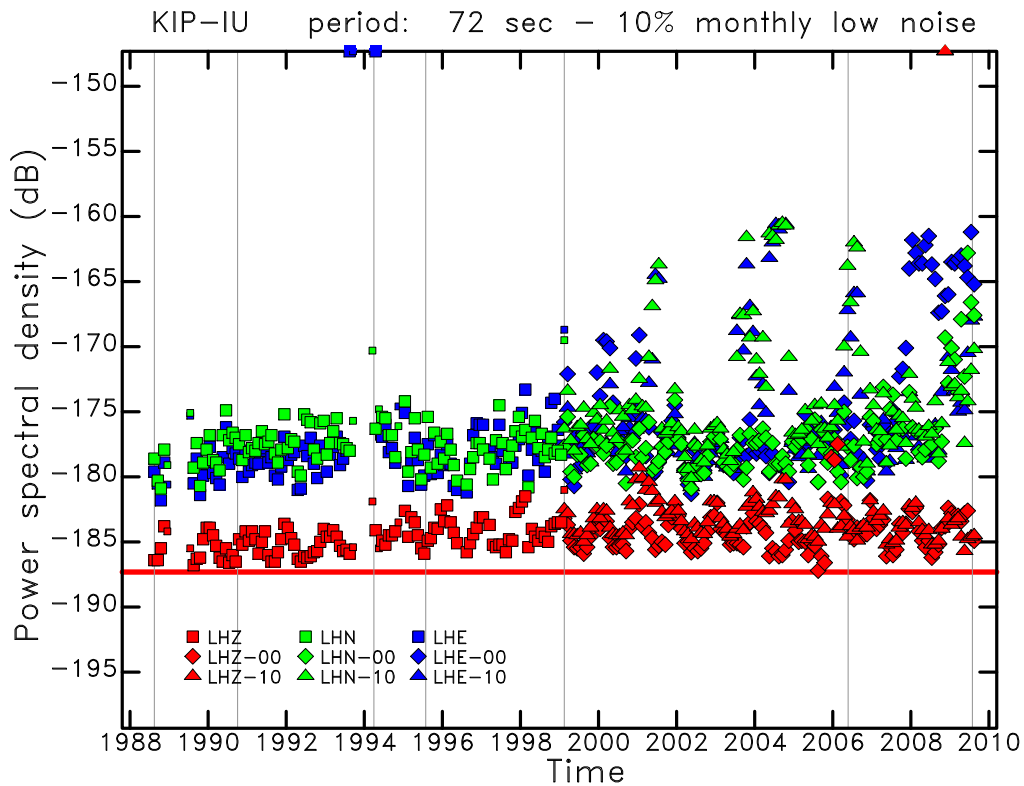


Figure 3: Monthly PSD of ground acceleration at 72-s period for all long-period (LH) channels at KIP for the period 1988–2009. Smaller symbols are used for months with fewer available hourly measurements. Each component and sensor is represented by a distinct symbol and color. The red horizontal line indicates the level of Peterson’s (1993) Low Noise Model (LNM) at 72 s. The thin vertical lines show the times of epoch boundaries in the station metadata.

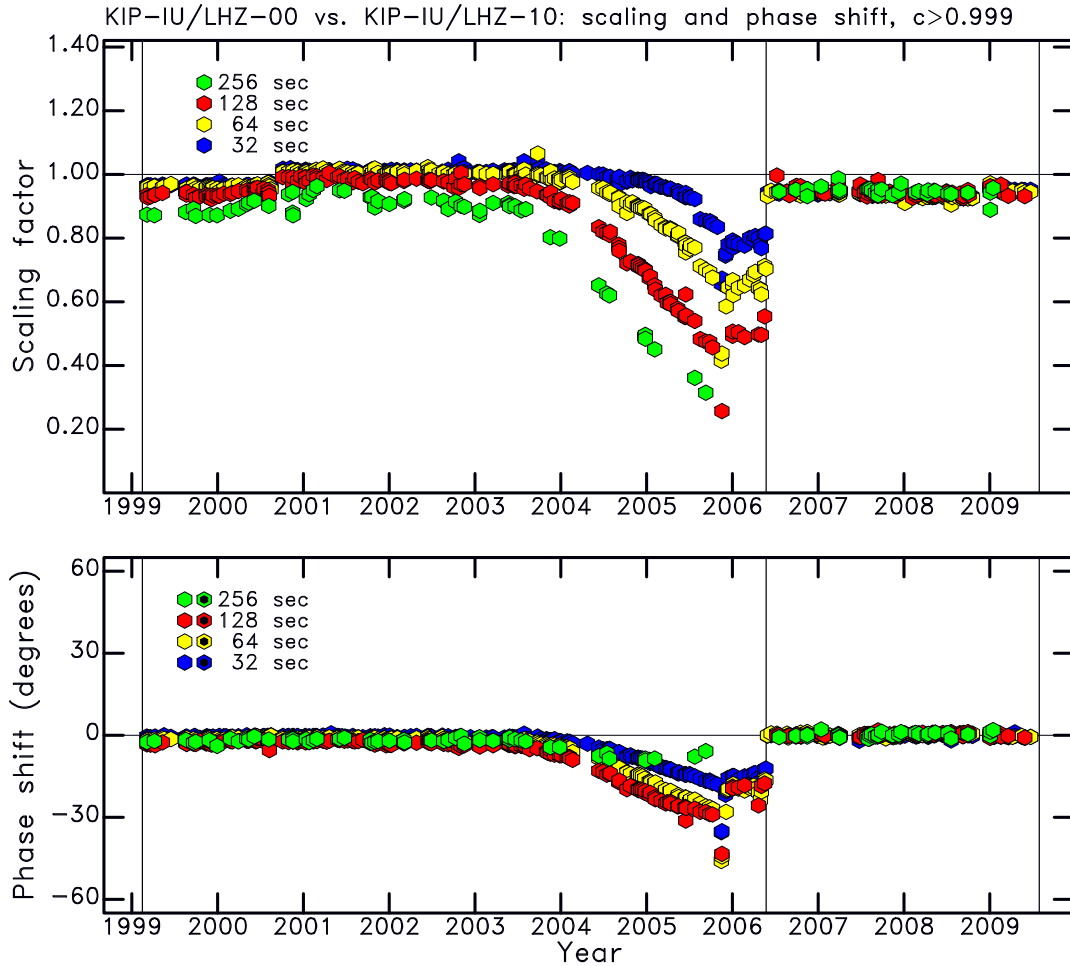


Figure 4: Diagram shows the result of coherence analysis for the vertical components of the STS-1 and STS-2 sensors. Each symbol represents a measurement of coherence for a $M_W \geq 6.5$ earthquake. The minimum coherence plotted is indicated by c . The scaling and phase between the two time series is shown at four different periods. The long-period gain is too small by $\sim 10\%$ in 1999 and the response function deteriorates with time. The instrument characteristics clearly change in 2006. The thin vertical lines show the times of epoch boundaries in the station metadata.

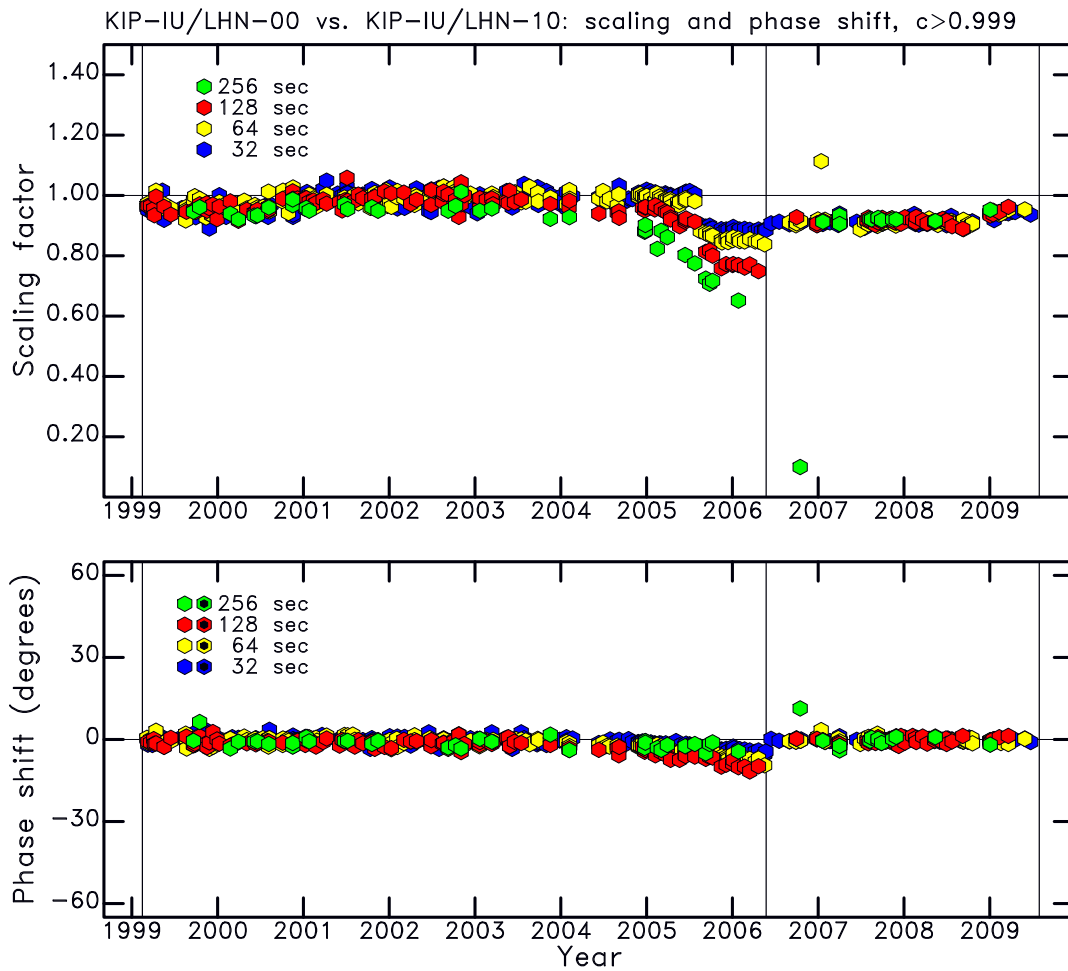


Figure 5: Same as Figure 4, but for the North-South components. A deterioration in the frequency response of the STS-1 sensor is evident during 2004–2006. A frequency-independent difference in gain of 5–10% with respect to the STS-2 is evident since 2006.

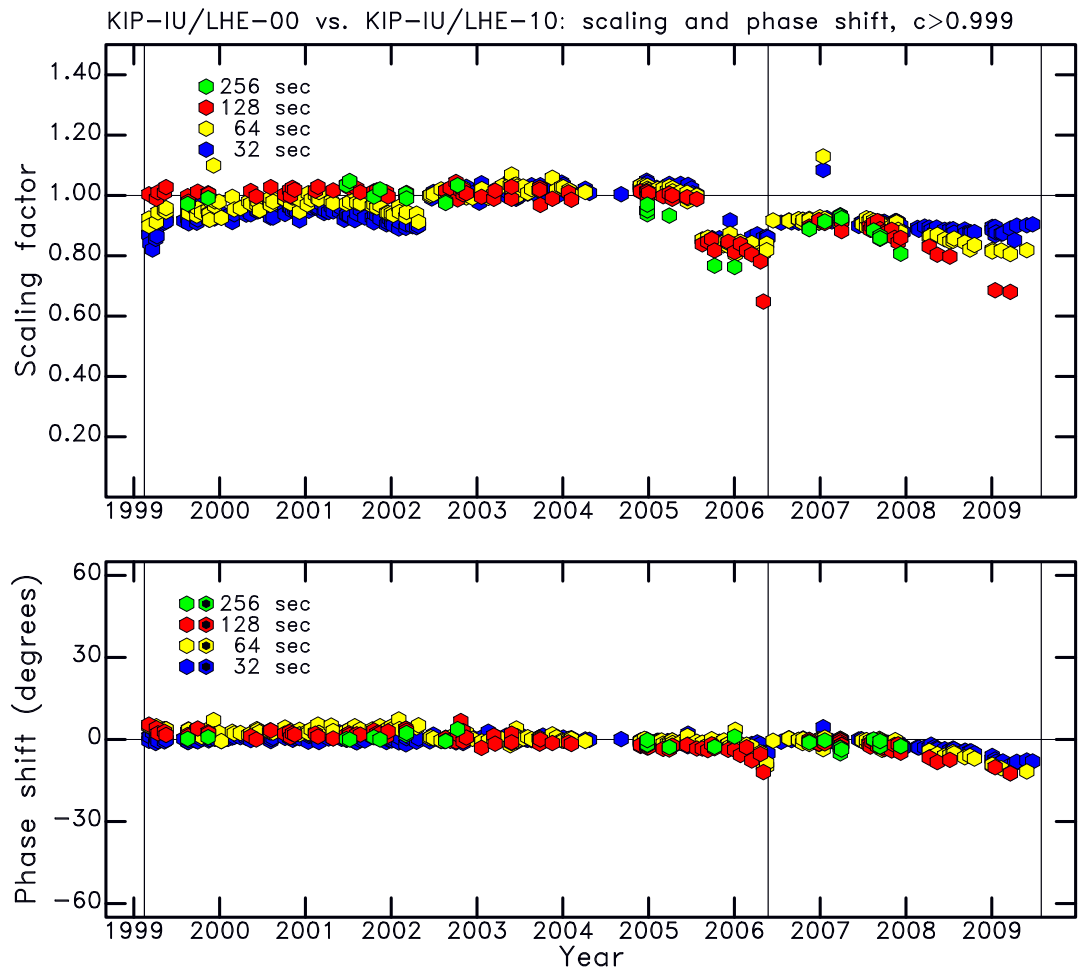


Figure 6: Same as Figure 4, but for the East-West components. The short-period gain is too small by 5–10% during 1999–2002, and a deterioration is seen in 2004–2006. The response appears to be deteriorating again following a slight recovery in 2006.

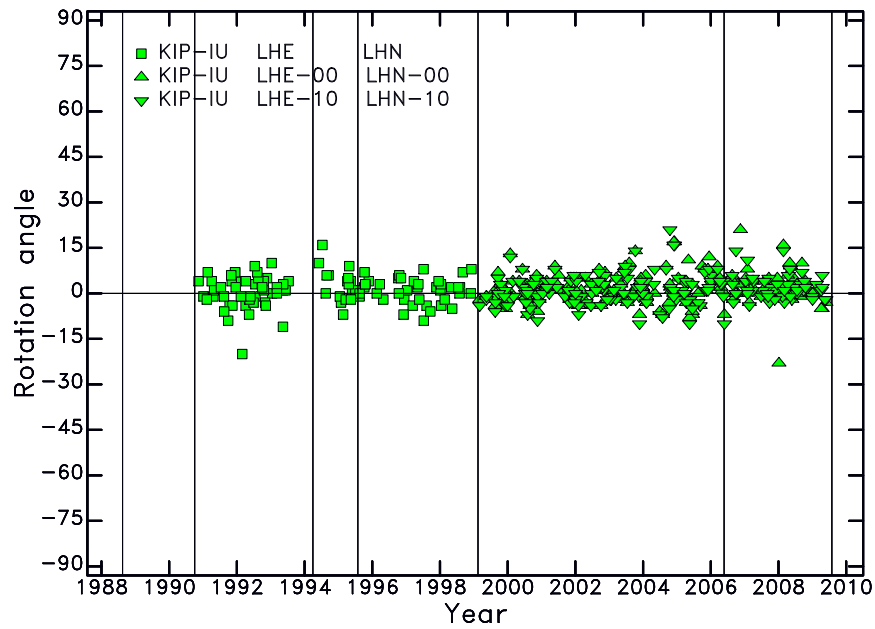


Figure 7: Individual measurements of polarization angle as a function of time. All measurements for the period of operation are shown. No measurements were possible in 1988–1989 since one or both horizontal components have reversed polarities (with respect to the those in the metadata) during this time period. Symbols represent measurements obtained in the surface-wave band of the CMT analysis. More than 50% of the observations lie in the range -2° to $+4^\circ$. The thin vertical lines show the times of epoch boundaries in the station metadata.

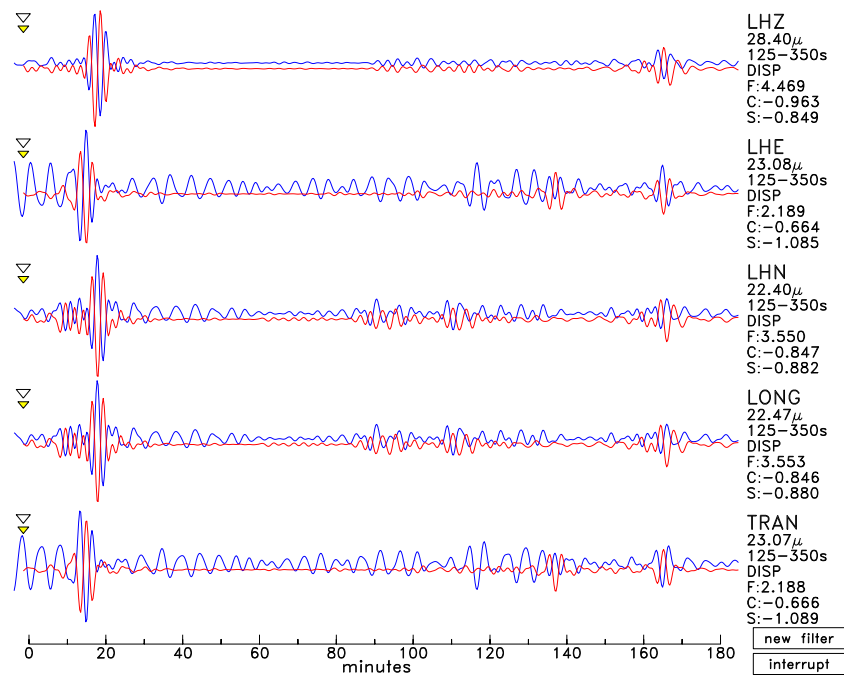


Figure 8: Comparison of observed (blue traces) and synthetic (red traces) mantle-wave seismograms for an earthquake on September 4, 1989. The channel name, maximum displacement, and values for the three parameters residual misfit (F), correlation (C) and scaling factor (S) are given to the right of each waveform. All channels are reversed in polarity with respect to the information in the metadata.

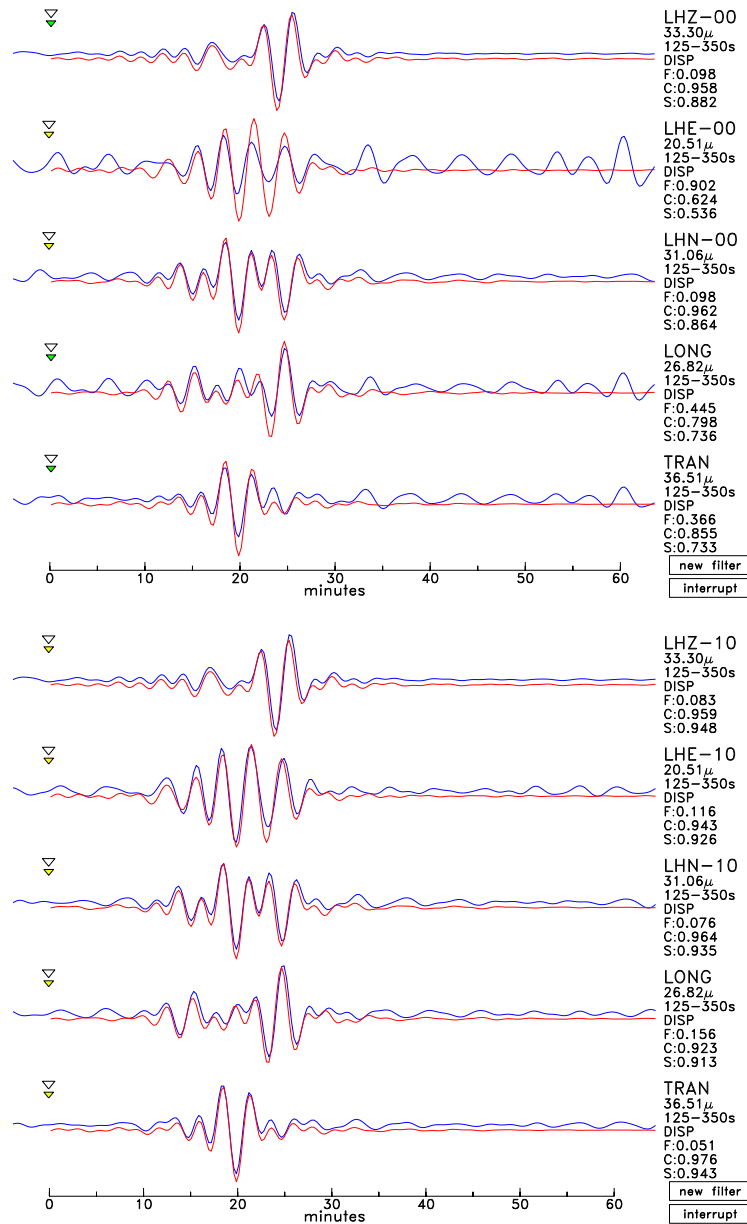


Figure 9: (Top) Observed (STS-1) and synthetic mantle-wave seismograms for an earthquake on April 7, 2009. The East-West component is poorly fit, reflecting the error in the response function evident in Figure 6. The problem is not only a difference in gain. (Bottom) Observed (STS-2) and synthetic body-wave seismograms for the same earthquake, but recorded on the STS-2 seismometer. The fit to all three components is good.